Title

Consensus recommendations for a dynamic susceptibility contrast MRI protocol for use in high-grade gliomas.

Journal

Neuro-Oncology, 22(9)

Authors

Boxerman, Jerrold
Quarles, Chad
Hu, Leland
et al.

Publication Date

2020-09-29

DOI

10.1093/neuonc/noaa141

Peer reviewed

Neuro-Oncology

22(9), 1262–1275, 2020 | doi:10.1093/neuonc/noaa141 | Advance Access date 9 June 2020

Consensus recommendations for a dynamic susceptibility contrast MRI protocol for use in high-grade gliomas

Jerrold L. Boxerman, Chad C. Quarles, Leland S. Hu, Bradley J. Erickson, Elizabeth R. Gerstner, Marion Smits, Timothy J. Kaufmann, Daniel P. Barboriak, Raymond H. Huang, Wolfgang Wick, Michael Weller, Evanthia Galanis, Jayashree Kalpathy-Cramer, Lalitha Shankar, Paula Jacobs, Caroline Chung, Martin J. van den Bent, Susan Chang, W.K. Al Yung, Timothy F. Cloughesy, Patrick Y. Wen, Mark R. Gilbert, Bruce R. Rosen, Benjamin M. Ellingson, and Kathleen M. Schmainda and the Jumpstarting Brain Tumor Drug Development Coalition Imaging Standardization Steering Committee

Department of Diagnostic Imaging, Warren Alpert Medical School, Brown University, Providence, Rhode Island, USA (J.L.B.); Department of Neuroimaging Research and Barrow Neuroimaging Innovation Center, Barrow Neurological Institute, Phoenix, Arizona, USA (C.C.Q.); Department of Radiology, Mayo Clinic, Rochester, Minnesota, USA (B.J.E., T.J.K.); Department of Neurology, Massachusetts General Hospital, Harvard Medical School, Boston, Massachusetts, USA (E.R.G.); Department of Radiology and Nuclear Medicine, Erasmus MC–University Medical Center Rotterdam, Rotterdam, Netherlands (M.S.); Department of Radiology, Duke University School of Medicine, Durham, North Carolina, USA (D.P.B.); Department of Radiology, Brigham and Women's Hospital, Boston, Massachusetts, USA (R.H.H.); Center for Neuro-Oncology, Dana-Farber/Brigham and Women's Cancer Center, Harvard Medical School, Boston, Massachusetts, USA (R.H.H., P.Y.W.); Department of Neurooncology, National Center of Tumor Disease, University Clinic Heidelberg, Heidelberg, Germany (W.W.); Department of Neurology, University Hospital and University of Zurich, Zurich, Switzerland (M.W.); Division of Medical Oncology, Department of Oncology, Mayo Clinic, Rochester, Minnesota, USA (E.G.); Martinos Center for Biomedical Imaging, Massachusetts General Hospital and Harvard Medical School, Boston, Massachusetts, USA (J.K.-C., B.R.R.); Division of Cancer Treatment and Diagnosis, National Cancer Institute (NCI), Bethesda, Maryland, USA (L.S., P.J.); Department of Radiation Oncology, The University of Texas MD Anderson Cancer Center, Houston, Texas, USA (C.C.); Department of Neuro-Oncology, Erasmus MC Cancer Institute, Rotterdam, Netherlands (M.J.v.d.B.); Department of Neurological Surgery, University of California San Francisco, San Francisco, California, USA (S.C.); Department of Neuro-Oncology, Division of Cancer Medicine, The University of Texas MD Anderson Cancer Center, Houston, Texas, USA (W.K.A.Y.); UCLA Neuro-Oncology Program and UCLA Brain Tumor Imaging Laboratory (BTIL), David Geffen School of Medicine, University of California Los Angeles, Los Angeles, California, USA (T.F.C., B.M.E.); Department of Neurology, David Geffen School of Medicine, University of California Los Angeles, Los Angeles, California, USA (T.F.C.); Neuro-Oncology Branch, National Cancer Institute (NCI), Bethesda, Maryland, USA (M.R.G.); Departments of Radiological Sciences, Psychiatry, and Biobehavioral Sciences, David Geffen School of Medicine, University of California Los Angeles, Los Angeles, California, USA (B.M.E.); Department of Biophysics, Medical College of Wisconsin, Milwaukee, Wisconsin, USA (K.M.S.); Department of Radiology, Mayo Clinic, Phoenix, Arizona, USA (L.S.H.); Representative of the Adult Brain Tumor Consortium (ABTC) (E.R.G., P.Y.W., B.M.E.); Representative of the Ivy Consortium for Early Phase Clinical Trials (B.M.E.); Representative of the Eastern Cooperative Oncology Group–American College of Radiology Imaging Network (ECOG-ACRIN) Cancer Research Group (J.L.B., D.P.B., B.M.E., K.M.S.); Representative of the European Organisation for Research and Treatment of Cancer (EORTC) (M.S., W.W., M.W., M.J.v.d.B.); Representative of the Alliance for Clinical Trials in Oncology (L.S.H., B.J.E., T.J.K., E.G., C.C.); Representative of the RSNA Quantitative Imaging Biomarker Alliance (QIBA) (B.J.E., D.P.B., B.M.E.); Representative of the American Society of Neuroradiology (ASNR) (J.L.B., L.S.H., B.J.E., D.P.B., B.M.E.); Representative of the American Society of Functional Neuroradiology (ASFNR) (J.L.B.); Representative of the Radiation Therapy Oncology Group (RTOG) (M.R.G.)

Corresponding Author: Jerrold L. Boxerman, MD, PhD Rhode Island Hospital, Department of Diagnostic Imaging, 593 Eddy Street, Providence, RI 02903 (jboxerman@lifespan.org).

Abstract

Despite the widespread clinical use of dynamic susceptibility contrast (DSC) MRI, DSC-MRI methodology has not been standardized, hindering its utilization for response assessment in multicenter trials. Recently, the DSC-MRI Standardization Subcommittee of the Jumpstarting Brain Tumor Drug Development Coalition issued an updated consensus DSC-MRI protocol compatible with the standardized brain tumor imaging protocol (BTIP) for high-grade gliomas that is increasingly used in the clinical setting and is the default MRI protocol for the National Clinical Trials Network. After reviewing the basis for controversy over DSC-MRI protocols, this paper provides evidence-based best practices for clinical DSC-MRI as determined by the Committee, including pulse sequence (gradient echo vs spin echo), BTIP-compliant contrast agent dosing (preload and bolus), flip angle (FA), echo time (TE), and post-processing leakage correction. In summary, full-dose preload, full-dose bolus dosing using intermediate (60°) FA and field strength-dependent TE (40–50 ms at 1.5 T, 20–35 ms at 3 T) provides overall best accuracy and precision for cerebral blood volume estimates. When single-dose contrast agent usage is desired, no-preload, full-dose bolus dosing using low FA (30°) and field strength-dependent TE provides excellent performance, with reduced contrast agent usage and elimination of potential systematic errors introduced by variations in preload dose and incubation time.

Keywords

cerebral blood volume | clinical trial | consensus protocol | DSC-MRI | high-grade glioma

In 1990, Rosen et al demonstrated transiently decreased brain signal intensity after bolus administration of gadolinium-based contrast agent (GBCA).[1] The signal intensity-time curve could be converted into a concentration-time curve, enabling voxel-wise computation of cerebral blood volume (CBV). This technique, now widely known as dynamic susceptibility contrast (DSC) MRI, uses the magnetic susceptibility properties of paramagnetic contrast agents (gadolinium chelates or superparamagnetic nanoparticles) and T2 or T2*-weighted acquisitions. DSC-MRI was used to perform the first "functional" MRI experiments of task-induced brain activation,[2] and produce the first MRI-based CBV maps of gliomas.[3]

Since these beginnings, studies have shown that DSC-MRI may be more useful than standard MRI at predicting treatment-naïve glioma grade[3–8] and survival,[9–13] distinguishing posttreatment pseudoprogression (PsP) and radiation necrosis from recurrent tumor,[14–17] and predicting response to anti-angiogenic therapy.[18–25] Use of DSC-MRI has consequently exploded over the past few decades, particularly in neuro-oncology. Geer et al found that the addition of DSC-MRI increased the confidence of neuroradiologists and treating physicians in their assessment of tumor status in 40% and 56% of cases, respectively, with treatment modification in 8.5% of patients,[26] highlighting the potential clinical impact of DSC-MRI. Despite this and other evidence for clinical impact on the management of brain tumor patients, technical aspects of DSC-MRI have not been standardized, which has hindered its widespread adoption and utilization for assessment of treatment response in multicenter therapeutic trials.

There are multiple protocol decisions for DSC-MRI that influence its practical implementation and the accuracy and precision of CBV measurement.[27] These include gradient echo (GRE) versus spin echo (SE) pulse sequence; contrast agent dosing, including preload and bolus; image acquisition parameters, including flip angle (FA), echo time (TE), temporal resolution (TR), and number of baseline and post-bolus data points; and post-processing techniques, including GBCA leakage correction. After reviewing the basis for controversy over DSC-MRI protocol, this study provides *evidence-based best practices for clinical DSC-MRI*, emphasizing our favored choices for these protocol decisions. The *evidence* comes from DSC-MRI theory, computer modeling, and simulation of DSC-MRI signal acquisition and post-processing, in vivo stereotactic tissue correlation, and single-institution and multisite clinical trial data. Because a primary goal for harmonizing DSC-MRI methodology is the facilitation of its widespread adoption and the collation of results from multisite trials, for *best clinical practice* we emphasize CBV *accuracy* and *precision* in neuro-oncology applications, including treatment response assessment of high-grade gliomas (HGGs) in clinical trials of novel therapeutics. Although advanced DSC-MRI methods including multi-echo approaches may measure additional features of tumor pathophysiology (including vessel caliber, vascular permeability, tumor cell size, and cytoarchitecture),[28,29] our recommendations focus on CBV measurement using single TE, GRE echo planar imaging and GBCA-based DSC-MRI, which is the most common methodology in practice and is concordant with other widely adopted brain tumor imaging protocols.[30]

A Brief Overview of DSC-MRI

DSC-MRI is based upon classical indicator dilution theory used by physiologists to quantitate hemodynamics of whole-organ systems from known quantities of injected non-diffusible tracers such as dyes and radiotracers, and

measurement of output tracer concentration.[31] DSC-MRI applies this methodology to the brain, using exogenous paramagnetic GBCA as the "tracer." DSC-MRI is a "bolus tracking" technique that rapidly acquires GRE or SE echo planar images before (baseline), during (bolus), and after (tail) first-pass transit through the brain of GBCA that transiently alters the acquired signal intensity.[32] Voxel-wise changes in relative contrast agent concentration are determined by converting the signal intensity-time curves into change in relaxation rate-time curves, assuming that transient signal loss is due solely to magnetic susceptibility effects resulting from the injected GBCA and the subsequent changes in T2* (GRE) or T2 (SE) relaxation rate ($\Delta R2^*$ and $\Delta R2$, respectively, and herein referred to collectively as $\Delta R2^*$ unless otherwise specified). Because $\Delta R2^*$ is assumed to be directly proportional to tissue GBCA concentration, with GBCA confined to the vasculature, the $\Delta R2^*$-time curves are processed using tracer kinetic modeling and indicator dilution theory to estimate cerebral hemodynamic parameters such as CBV, cerebral blood flow (CBF), and mean transit time (MTT).[1] Absolute CBV can theoretically be determined from the area under the $\Delta R2^*$-time curve normalized to the integrated arterial input function (AIF).[33] Most often, to avoid the well-known difficulties of accurately determining the AIF, relative CBV (rCBV) is estimated from the area under the $\Delta R2^*$-time curve alone giving a CBV value that has meaning relative to other parts of the brain. For comparison across time and patients, rCBV may be normalized to rCBV in normal-appearing white matter, yielding the most common DSC-MRI metric for evaluating brain tumors, normalized rCBV (nRCBV). Alternative methods precluding the need to normalize rCBV to reference brain include standardization and Gaussian normalization.[34,35]

Basic Contrast Mechanism for DSC-MRI

The DSC-MRI contrast mechanism is based upon compartmentalization of paramagnetic GBCA that establishes magnetic susceptibility difference between the intra- and extravascular space, creating magnetic field gradients.[32] Protons lose phase coherence as they diffuse through the transient, spatially varying gradients, yielding signal attenuation dependent upon physiological factors, including vessel or compartment size and proton diffusion rate, and experimental factors, including pulse sequence parameters and contrast agent concentration.[36] Although this behavior can be solved analytically for limited regimes, this phenomenon has been most generally studied using Monte Carlo numerical methods that quantify the relationship between change in relaxation rate and the physiological and experimental parameters.[36,37] These simulations yield the vessel size-dependence relationships for GRE ($\Delta R2^*$) and SE ($\Delta R2$) change in relaxation rate, with $\Delta R2^*$ plateauing for large diameter vessels, and $\Delta R2$ peaking for capillary-sized vessels. (eg, Figure 1 in Reference[36]). These relationships are qualitatively independent of vessel geometry.

Gradient-Echo versus Spin-Echo Acquisitions

The vessel size-dependence relationships have clinical implications. Because $\Delta R2$ peaks for microvessels, SE DSC-MRI is advantageous in stroke imaging aimed at

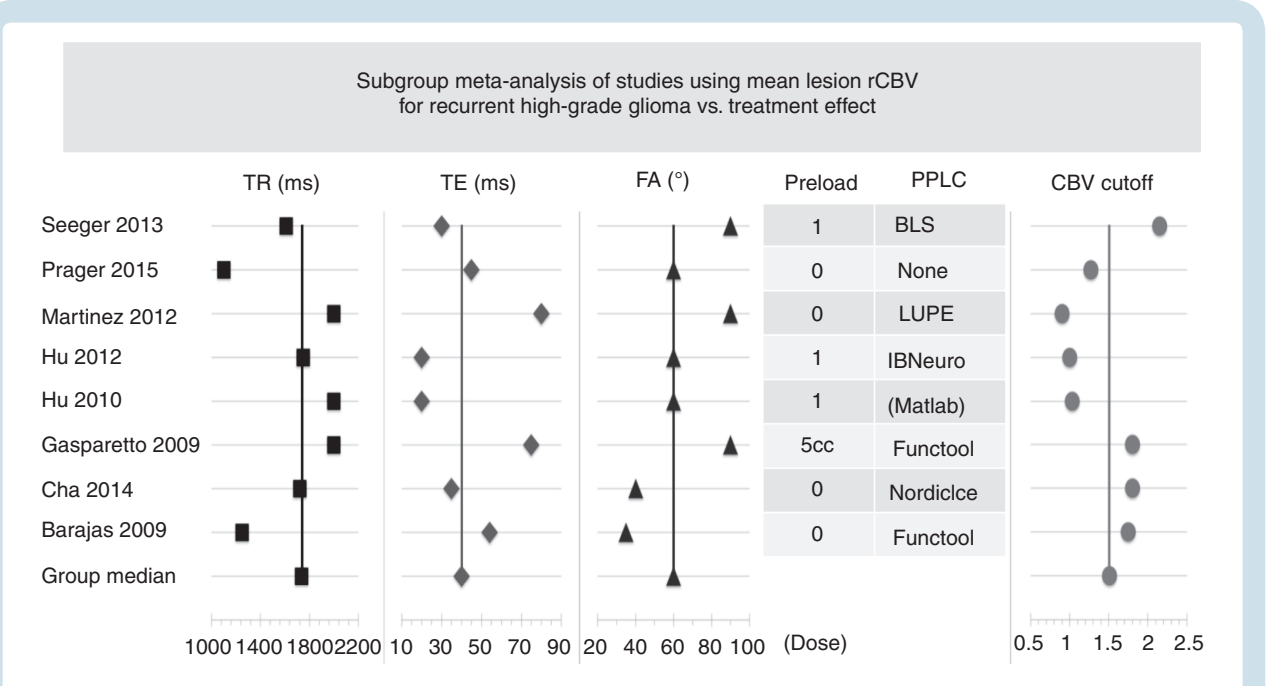

Fig. 1 DSC-MRI methodology in the literature varies greatly, as seen in the subgroup meta-analysis by Patel et al of studies using mean lesion rCBV for recurrent high-grade tumor vs treatment effect. These studies used a wide range of DSC-MRI parameters including TE, FA, preload dose, and post-processing leakage correction (PPLC).[79]

identifying capillary-level perfusion deficits,[38] with reduced blooming artifact in cortex around sulcal vessels. GRE DSC-MRI is sensitive to the larger, disorganized vessels that characterize HGGs,[39,40] with obvious application to tumor imaging. For given contrast agent concentration, field strength, and imaging parameters, ΔR2* exceeds ΔR2 for all vessel sizes, with larger corresponding signal loss.[36] Therefore, GRE-derived CBV maps have higher inherent signal-to-noise ratio (SNR) and sensitivity than SE CBV maps, and can provide greater signal changes for equal GBCA dose, or equivalent signal changes with lower GBCA dose, compared with those derived with SE DSC-MRI.

In order for DSC-MRI to accurately measure cerebral hemodynamics, there must be a linear relationship between change in relaxation rate and GBCA concentration. From basic susceptibility contrast principles, change in relaxation rate is directly proportional to GBCA concentration only where the ΔR2 or ΔR2* versus vessel size curves are "plateaued."[41] This plateau occurs over a much broader range of vessel sizes for GRE (ΔR2*) compared with SE (ΔR2) DSC-MRI, and so GRE CBV estimates are inherently more accurate than SE CBV estimates. Similarly, the *x*-axis of the size-dependence curves actually scales as R^2/D, where R is the vessel size and D is the proton diffusion rate.[41] Therefore, decreasing D (restricted diffusion) has the same effect as increasing vessel size (moving to the right on the change in relaxation rate versus vessel size graphs). While increasing vessel diameter or decreasing diffusion can result in either increased or decreased ΔR2, ΔR2* will be much less affected because of the plateau in the ΔR2*-size curve. Therefore, in tumors with heterogeneous proton diffusion and abnormal vascular morphology, hyperintensity on CBV maps is more likely to reflect truly elevated blood volume for GRE acquisitions versus greater uncertainty for SE acquisitions.

For these reasons—sensitivity to larger, disorganized microvessels seen in higher-grade tumors; greater signal changes for a given contrast agent dose; greater inherent accuracy of CBV estimates; and decreased sensitivity to changes in proton diffusion—GRE DSC-MRI is recommended for neuro-oncology applications. Thus, moving forward, we will only refer to T2* changes that occur with GRE DSC-MRI.

Consequences of Contrast Agent Extravasation

Another requirement for DSC-MRI to mimic tracer kinetics is that contrast agent must remain intravascular, which is violated for GBCAs in HGGs with blood–brain barrier (BBB) disruption and avid contrast enhancement. GBCA extravasation results in T1 shortening, opposing the susceptibility contrast induced T2* relaxation rate change from intravascular GBCA that forms the basis for CBV estimation. Because GBCA is excluded from cells, GBCA extravasation establishes a magnetic susceptibility gradient not only between the intra- and extravascular spaces, but also between the intra- and extracellular spaces when sufficient GBCA distributes throughout the extravascular-extracellular space, potentially exaggerating T2* changes. In the same voxel, the post-bolus signal can overshoot or undershoot baseline depending upon the accumulated dose of GBCA. (see for example Figure 5 in Reference[42].) DSC-MRI signal is thereby affected not only by vascular volume fraction and vessel size, but also by the rate of GBCA extravasation (vascular permeability) and the cell volume fraction, cell size, and cell distribution.[28] Signal-time (and ΔR2*-time) curves no longer return to baseline as they do for ideal tracer kinetics, but extend below or above baseline depending on whether T1 or T2* effects dominate, thereby affecting the accuracy of CBV estimates determined from the area under the ΔR2*-time curve.[43] The magnitude of this effect depends upon a combination of both DSC-MRI acquisition parameters and contrast agent dosing.[42]

Methods for minimizing DSC-MRI signal contamination from GBCA extravasation include low FA pulse sequences that reduceT1 sensitivity,[44] loading doses or "preload" contrast administration,[5,8,45] and post-processing techniques, including model-based leakage correction that can rectify both T1 and T2* leakage effects.[5,8,45–47] Dual-echo DSC-MRI utilizes 2 GRE acquisitions with different TEs to estimate change in relaxation rate directly, thereby eliminating T1 contamination effects entirely, but still requires correction for T2* leakage effects[48] and special pulse sequences that are less widely available.[38,49] No technique has been universally accepted, and much of the debate about best DSC-MRI methodology centers on issues related to minimizing contamination of the DSC-MRI signal due to GBCA extravasation and maximizing CBV accuracy.

Intravascular contrast agents like ferumoxytol eliminate contrast agent leakage effects entirely, and there is compelling evidence that ferumoxytol-based CBV measurements are inherently more accurate and precise than gadolinium-based CBV measurements because complications related to GBCA extravasation are minimized.[50] However, clinical application of ferumoxytol-based DSC-MRI may be limited. FDA-approved as a therapeutic iron supplement, ferumoxytol is less commonly available than GBCA for MRI. GBCAs are widely accepted by radiologists for conventional post-contrast imaging, and adding a second contrast agent for DSC-MRI would be logistically challenging. Although conventional contrast-enhanced imaging is feasible with ferumoxytol, it is practically performed 24 hours after agent administration.[51] Furthermore, the standardized brain tumor imaging protocol (BTIP) requires post-contrast imaging after one total dose of GBCA.[30] Finally, gadolinium-based DSC-MRI permits measurement of additional physiological parameters related to GBCA extravasation, such as percent signal recovery (PSR) of the signal-time curve compared with baseline, as well as K^{trans} (volume transfer coefficient of gadolinium from the intravascular to the extravascular, extracellular space). Therefore, we focus on single-GRE GBCA-based DSC-MRI and the selection of four fundamental protocol choices: preload and bolus contrast agent dose, FA, TE, and post-processing leakage correction.

Preload Contrast Agent Dosing

A "preload" dose of GBCA administered prior to the bolus dose of GBCA given during dynamic imaging can help

mitigate T1 contamination. The preload dose partially saturates baseline T1-weighted signal contribution,[5,8,45] thereby diminishing T1-induced increased signal during bolus passage. Evidence supporting preload administration includes data in a C6 rat glioma model, where (at least for high-FA acquisitions) there is no discernible DSC-MRI signal after the first (no preload) injection, and a "usable" DSC-MRI signal for computing CBV with the second injection.[46] A study comparing several different approaches for acquiring and computing rCBV maps in patients demonstrated that without preload, high-grade tumor may mistakenly show no rCBV elevation compared with normal brain, but expected rCBV elevation is found when a preload was used.[42] Preload dosing has varied in the literature, ranging from fractional doses up to a full equivalent dose. In a study using a 60° FA and post-processing leakage correction, Hu et al found that a full-dose preload of 0.1 mmol/kg and an incubation time of 6 minutes between preload administration and bolus injection optimized the separation of CBVs for tumor and treatment effect in HGGs with recurrent enhancement after standard chemoradiation.[52]

Post-Processing Leakage Correction

In practice, DSC-MRI acquisition cannot be decoupled from post-processing, and there is ample evidence that post-processing leakage-correction of DSC-MRI data is necessary for accurate rCBV measurement when the BBB is disrupted.[5,8,45] A pharmacokinetic model-based approach described by Weisskoff et al[53] was the first published method for correcting T1-based GBCA leakage effects using a linear least-squares fit of the $\Delta R2^*$-time curves within the tumor and a reference region in non-enhancing brain to correct the entire $\Delta R2^*$-time curve, including first pass.[5,8,45,46] The method was subsequently modified to correct T2* leakage effects as well,[45,54] and it was empirically determined that the algorithm performed best with the collection of 120 time points, a finding consistent with the assumption of no contrast agent backflux. This leakage correction method is now sometimes referred to as the BSW method (after the authors of the subsequent paper that focused exclusively on the leakage correction algorithm[8]).

Modifications to the BSW approach have since been published, including calculation of the tissue residue function allowing for a voxel-wise correction of the raw DSC-MRI signal that is insensitive to variations in MTT.[46] The ability to determine additional perfusion parameters directly from the residue function has also been demonstrated.[54] Most recently, a "bidirectional" version of the BSW method was developed that accounts for backflux of contrast agent,[47,55] which becomes important with the collection of >120 time points. While other leakage correction methods like gamma-variate fitting and post-bolus baseline correction have been used, studies suggest that these do not perform as well because they do not correct for leakage effects occurring throughout the DSC-MRI bolus.[42,46]

Preload and model-based post-processing leakage correction are synergistic in their improvement of rCBV accuracy,[42] and consensus recommendations for leakage-corrected, single-echo DSC-MRI have been directed toward a technique combining the two methods.[56] For high FA, rCBV using preload plus leakage correction strongly correlates with tumor grade, whereas uncorrected rCBV does not,[8] and in a rat gliosarcoma model, combined preload and post-processing leakage correction yield CBV estimates that converge to gold standard values obtained using MION (monocrystalline iron oxide nanoparticle), an intravascular contrast agent.[57] Relative CBV measurements using preload and the BSW method agree well with histology in spatially correlated tissue biopsies,[58,59] and the BSW method has been applied in single-institution studies and multisite clinical trials demonstrating, among other benefits, the utility of rCBV for predicting or detecting early responses to therapy.[20,23,60,61] Nonetheless, there are potentially important improvements to be gained using modified BSW approaches that have yet to be thoroughly evaluated.

Although the BSW method has been implemented by several commercial software vendors, discrepancies in computed rCBV arise in head-to-head comparisons,[62] and caution is recommended for cross-platform comparisons. For instance, significantly different performance was observed when identical DSC-MRI data were processed with 2 software packages using different implementations of post-processing leakage correction.[62] The best correlation of CBV with histology required preload plus post-processing leakage correction, providing evidence that leakage correction is important but that technique and implementation matter. Marked intersite disagreement has also been observed when site-specific software was applied to DSC-MRI data generated by a digital reference object (DRO) using a standardized imaging protocol.[63] Nonetheless, it has been shown that when a single dataset is carefully pre-processed eliminating differences in intermediate analysis steps (such as region-of-interest selection and registration), then rCBV values computed by multiple sites using different platforms begin to converge,[64] and a "consensus" threshold is reached for distinguishing low-grade from high-grade gliomas. Therefore, implementation matters, motivating efforts to build consensus regarding post-processing and to establish a benchmark for validating DSC-MRI analysis tools, such as the DRO described below.[65,66]

Impact of Flip Angle and TE

For single-echo DSC-MRI, low to intermediate FA (ie, 35°–60°) with longer TR (ie, 1.2–1.7 s) and TE (ie, >20 ms) can reduce T1 contamination due to GBCA extravasation.[44] However, some parameter combinations may also reduce the SNR of the computed rCBV maps,[67] and the goal is to minimize leakage effects while maintaining SNR. Accordingly, there are high- and low-FA DSC-MRI strategies with tradeoffs, as summarized in Table 1. Acquisitions using low FA,[44] long TE,[68] and long TR[69] have decreased T1 sensitivity, and less need for preload, but poorer CBV SNR. Higher FA,[8] shorter TE,[70] and shorter TR[67] may require preload to decrease T1 sensitivity, but have higher CBV SNR.

We have direct validation of CBV accuracy using 2 different acquisition strategies. Stereotactic biopsies

Table 1 Summary of CBV SNR and T1 sensitivity tradeoffs for DSC-MRI acquisition strategies

Acquisition Parameters			
Parameter	CBV SNR	T1 sensitivity	Reference
Flip angle			
Low	Decrease	**Decrease**	Cha et al. Radiology 2002[44]
High	**Increase**	Increase	Boxerman et al. AJNR 2006[8]
TE			
Long	Decrease	**Decrease**	Thilmann et al. MRI 2004[68]
Short	**Increase**	Increase	Smith et al. MRM 2003[70]
TR			
Long	Decrease	**Decrease**	Knutsson et al. MRI 2004[69]
Short	**Increase**	Increase	Boxerman et al. JMRI 1997[67]
Preload contrast agent administration			
Pros	**Cons**	**Reference**	
Decreased T1 sensitivity	Extra contrast agent	Donahue et al. MRM 2000[5]	
	Variable incubation time	Hu et al. AJNR 2010[52]	

co-registered to leakage-corrected CBV maps made with preload, 60° FA, and post-processing leakage correction have shown excellent correlation of CBV with histologic vascular area and density.[58] Similarly, stereotactic biopsies co-registered to CBV maps made using no preload, a low FA (35°), and no model-based leakage correction also had good correlation of CBV with microvascular expression.[71] The literature is replete with conflicting acquisition strategies such as these.

Motivation for Standardization of DSC-MRI Methodology

The application of DSC-MRI to treatment response assessment of HGGs illustrates the importance of harmonization of DSC-MRI methodology. There has been much investigation of the use of CBV for differentiating true tumor from treatment effects. Relative CBV has putative value for differentiating progressive disease (PD) characterized by enlarged microvessels with high vascular density from treatment effects characterized by inflammatory or steroid-like behavior as in PsP or pseudoresponse, respectively.[72–74]

CBV has been used to distinguish PsP and PD at initial progressive contrast enhancement after chemoradiation but the literature is somewhat conflicting. For instance, Prager et al studied 68 HGGs at progressive enhancement and found significant difference in median rCBV between PsP and PD, with an optimal threshold of 1.3.[75] Other studies also found mean or median CBV to be predictive, with varying thresholds,[19,76] but others have found mean CBV to be non-predictive or only predictive with qualification. Although Kong et al found overall significant difference in mean rCBV between PsP and PD, this difference applied to glioblastomas (GBMs) with unmethylated but not with methylated O^6-methylguanine-DNA methyltransferase.[77] However, a study of HGGs treated with PPX (paclitaxel poliglumex), a powerful radiation sensitizer with a high incidence of PsP often coincident with PD, found no significant difference in mean rCBV between PsP and PD at initial progressive enhancement.[78] These are just a few examples of varied results in the literature.

Variability of DSC-MRI Methodology in the Literature

Literature results may conflict at least in part because DSC-MRI methodology varies greatly. Patel et al published a meta-analysis of 17 studies where DSC-MRI was used to differentiate recurrent HGG from treatment-related enhancement.[79] For the subgroup of studies using mean lesion rCBV, they found "relatively good accuracy in individual studies" with high pooled sensitivity (88% [0.81–0.94]) and specificity (88% [0.78–0.95]) for recurrent tumor, but there was a wide range of optimal mean CBV thresholds (0.9–2.15). This variation has been attributed to the wide range of TR, TE, FA, preload dose, and post-processing leakage correction used by these studies, as summarized in Fig. 1. Variable parameters are also found in subsequent literature. For instance, using spatially correlated histologic tissue samples, TR = 1100–1250 ms, TE = 30 ms, FA = 70–80°, ½–1 dose preload with full-dose bolus, and post-processing leakage correction (IB Neuro), Prah et al found nRCBV cutoff of 1.13 with 82% sensitivity and 90% specificity.[59] Patel et al concluded that "because of significant variability in optimal reported thresholds . . . further investigation and standardization is needed before implementing any particular quantitative PWI [perfusion weighted imaging] strategy across institutions."

On a similar note, Quarles et al organized a Quantitative Imaging Network (QIN) DSC-MRI challenge with 12 NCI-QIN centers to explore factors related to CBV consistency.[63]

They simulated a 10000-voxel population-based DRO for each site's DSC-MRI protocol (19 total protocols),[65] and used corresponding DSC-MRI signal curves for 3 evaluations of intersite CBV consistency: central processing of CBV for site-specific DROs (isolated impact of acquisition protocol); site-specific processing of CBV for standard DRO (isolated impact of post-processing methodology); and site-specific processing of CBV for site-specific DROs (combined impact of acquisition and post-processing). The 3T DSC-MRI acquisition protocol varied considerably for the 12 sites (15 paradigms). Though TR and TE were relatively consistent (possibly reflecting adoption of previously published protocol recommendations[56]), FA and preload dosing varied considerably, with a wide gamut of post-processing methodology, including software, integration limits, and normalization to white matter. When local sites chose both acquisition and post-processing, there was very poor cross-site intraclass correlation for CBV, particularly for simulated BBB disruption typical for GBMs, and with large limits of agreement on Bland–Altman analysis. There was better correlation when acquisition or post-processing was standardized, especially post-processing. Overall, this study demonstrates that CBV variability can arise from differences in post-processing as well as image acquisition. This has profound implications for comparing literature CBV values from sites using dissimilar acquisition and post-processing schemes. For clinical trials, although acquisition and post-processing methods are typically standardized, the most accurate and proven approaches should be used for determining the therapeutic effectiveness of a drug or establishing thresholds for categorical response (eg, predetermined changes in CBV used to refine Response Assessment in Neuro-Oncology criteria).

Previous Efforts at Standardization: American Society of Functional Neuroradiology White Paper (2015)

Efforts at standardization have been made by several organizations, including the American Society of Functional Neuroradiology (ASFNR), which published a white paper with the following recommendations: single-echo, GRE pulse sequence; TR = 1.0–1.5 s; TE = 40–45 ms at 1.5T, 25–35 ms at 3T; FA = 60–70°; acquisition duration of at least 120 total time points, including at least 30–50 baseline acquisitions; and ¼–1 dose preload with full-dose bolus.[56] These recommendations were made prior to the publication of the standardized BTIP,[30] which is gaining clinical acceptance.

BTIP Compliance and Implication for Allowable Dosing Schemes

It is sensible that a standardized DSC-MRI protocol be compatible with BTIP. BTIP mandates that conventional post-contrast T1-weighted imaging be performed after one full dose of GBCA, either split between preload and DSC-MRI bolus before post-contrast imaging or fully given as preload with variable bolus dose DSC-MRI after post-contrast imaging. This sets constraints on the range of preload and bolus doses that should be considered for inclusion in a universal DSC-MRI protocol. Possible BTIP-compliant DSC-MRI preload and bolus paradigms are illustrated in Fig. 2.

Selection of Optimal DSC-MRI Parameters: Computational Approach

Because it is impractical to compare all possible acquisition schemes in vivo, computational approaches have been pursued for determining optimal acquisition parameters.

Using a multicompartment model-based simulation of DSC-MRI signal derived from convolution theory,[80] the theoretical framework developed by Quarles et al,[43] and characteristics from 250 randomly chosen tumors, Leu et al systematically evaluated the effects of various acquisition and post-processing leakage correction strategies, including a range of FA, TE, and TR with BTIP-compliant contrast agent dosing schemes, on the fidelity of CBV estimation in the presence of Gaussian noise.[81] Results of this comprehensive study are summarized in Fig. 3. Although no single acquisition scheme was absolutely optimal, several parameter combinations yielded the lowest error in CBV estimation. The best performing acquisition schemes included 60° FA with full-dose preload and full-dose bolus ("1 + 1" double-dose GBCA), as well as 35° FA without preload. Importantly, high-FA acquisitions with no or fractional preload dosing performed relatively poorly.

Similarly, Semmineh et al used a validated population-based DRO, derived from 3D tumor tissue microstructures and trained on 23 DSC-MRI GBM datasets including more than 40000 voxels.[65] They simulated tumor CBV acquired with BTIP-compliant dosing schemes, and a similar range of FA, TE, and TR. Simulated CBV without leakage was the reference standard, and they evaluated concordance correlation coefficient and coefficient of variation as measures of accuracy and precision, respectively. They produced heat maps with similar findings as Leu et al. The best performing schemes used full-dose preload and full-dose bolus at low to intermediate FA, with poor performance for intermediate-high FAs using no or fractional preload, particularly at 1.5 T.[66] Confluent regions of high performance are desirable because these schemes would presumably be less sensitive to minor parameter variations or to underlying model assumptions or tumor physiology.

Fig. 4 summarizes performance of the intermediate 60° FA scheme from the ASFNR white paper versus a high-performing, low FA scheme for TR = 1.5 s. Full-dose preload with full-dose bolus ("1 + 1" double-dose GBCA) provides the highest accuracy and precision for both schemes with similar performance at 1.5 and 3 T. With intermediate FA, single total dose schemes have poorer performance, especially at 1.5 T, with moderate performance for split dose at 3 T. Low FA acquisitions give much better performance for single total dose. For single-dose contrast without preload,

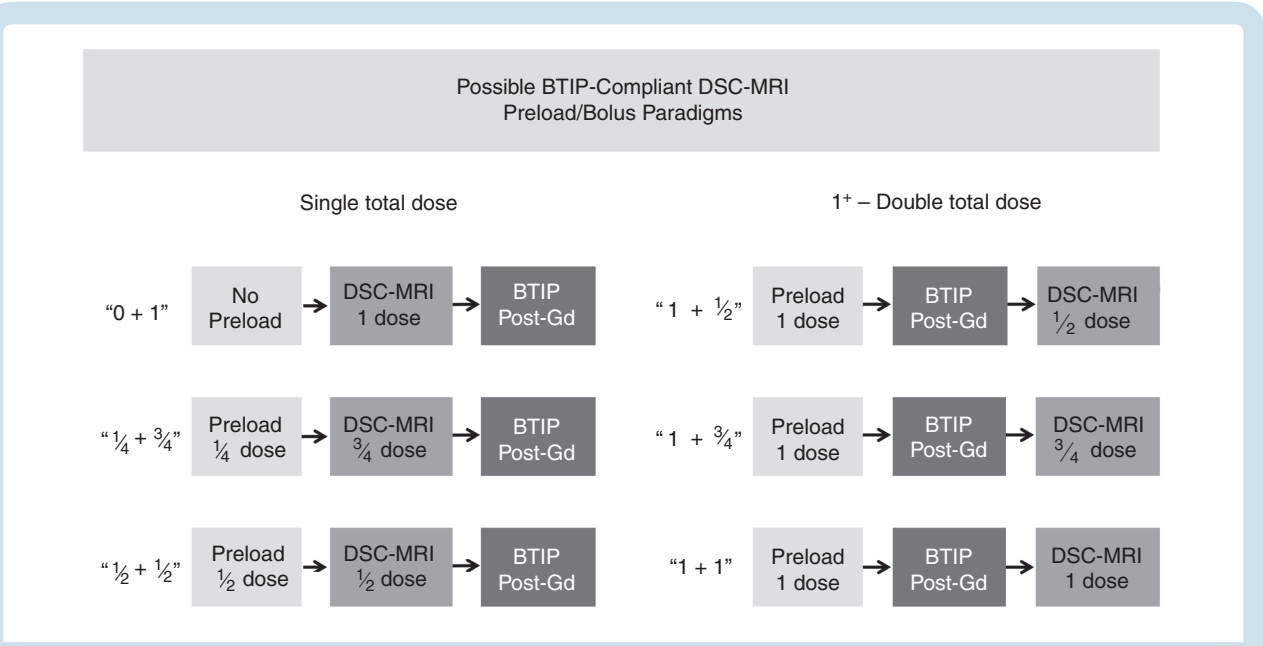

Fig. 2 Possible BTIP-compliant DSC-MRI preload + bolus dose paradigms. Either a single total dose must be split between preload and DSC-MRI before post-GBCA imaging or a full dose preload must be given with DSC-MRI after post-contrast imaging.

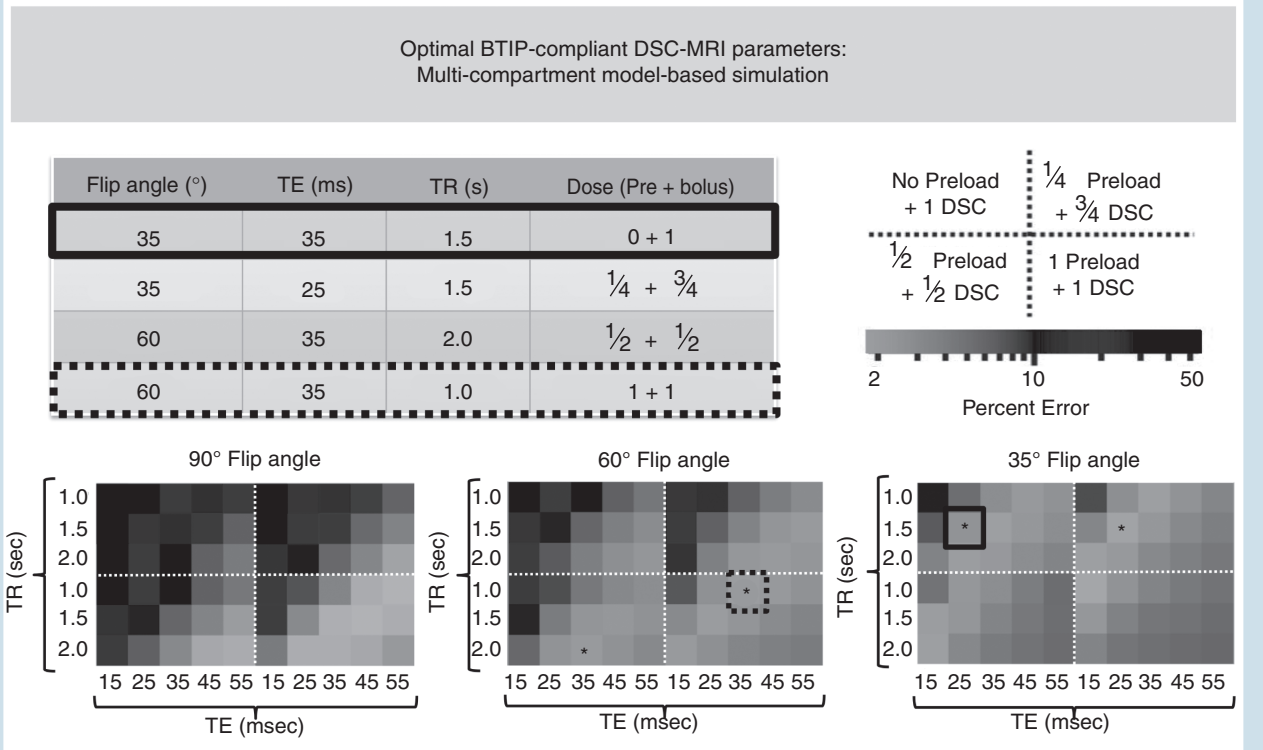

Fig. 3 Computational approach for determining optimal BTIP-compliant DSC-MRI parameters using simulated DSC-MRI signal with GBCA leakage: heat maps of CBV error versus theoretical CBV without leakage for different combinations of acquisition parameters. Schemes with particularly high fidelity at 3T include 60° FA with full-dose preload and bolus (asterisk with dashed box) and low FA without preload (asterisk with solid box).[81]

Optimal BTIP-compliant DSC-MRI parameters:
comparison of low FA and intermediate FA acquisitions

		Intermediate flip angle (ASFNR white paper) FA = 60°, TE = 30ms, TR = 1.5s				Low flip angle 1.5T: FA = 30°, TE = 50ms, TR = 1.5s 3.0T: FA = 30°, TE = 30ms, TR = 1.5s			
	Dosing (PLD + Bolus)	1.5 T		3T		1.5 T		3T	
		CCC	CV (%)	CCC	CV (%)	CCC	CV (%)	CCC	CV (%)
BTIP-compliant	1 + 1	0.92	7.4	0.97	6.6	0.96	7.4	0.98	6.8
	½ + ½	0.44	16.3	0.76	9.2	0.89	10.8	0.90	8.7
	¼ + ¾	0.38	18.2	0.74	8.8	0.91	9.0	0.94	7.8
	0 + 1	0.12	41.4	0.55	12.4	0.85	9.3	0.92	8.2
Non-BTIP	¼ + 1	0.72	8.2	0.93	6.8	0.95	7.7	0.97	7.0
	½ + 1	0.87	7.8	0.96	6.8	0.95	7.5	0.97	6.8

Fig. 4 Computational approach for determining optimal BTIP-compliant DSC-MRI parameters using a digital reference object matched to glioblastoma training data: performance comparison for intermediate and low flip angle schemes. For double-dose contrast with full-dose preload, both schemes have excellent accuracy and precision at 1.5T and 3T. For single-dose contrast without preload, intermediate FA performs poorly but low FA maintains excellent performance, even at 1.5T. For each dosing scheme, low FA had equal or better performance than intermediate FA. CCC = Concordance correlation coefficient (accuracy); CV = coefficient of variation (precision).[66]

the ASFNR parameters (ie, intermediate FA) perform poorly, but low FA maintains excellent performance, even at 1.5 T. Non-BTIP compliant preload dosing (eg, ½ dose, ¼ dose) with full-dose bolus can give excellent results with low FA and intermediate FA at 3 T, and very good results at 1.5 T.

Convergence of results from these simulations suggest that even without preload (ie, "0 + 1" dosing), a low FA scheme gives very accurate CBV with much less bias compared with intermediate FA, even at 1.5 T, and could be an attractive approach requiring less contrast agent (Fig. 5A).

With the application of simultaneous multislice or multiband techniques, it is possible to shorten the temporal resolution to subsecond TRs, while maintaining sufficient spatial coverage. DRO-based recommendations for TR, TE, and FA seek the optimal T1 and T2* sensitivity, and subsecond TRs will increase sensitivity to T1 leakage effects and reduce rCBV fidelity. For example, the DRO analysis for "0 + 1" dosing and the optimal low FA approach described above (30° FA, 30 ms TE) predicts that the concordance correlation coefficient (CCC), a measure of CBV accuracy, drops to 0.76 and 0.62 for TR = 750 ms and 500 ms, respectively. Even if TE is increased to 50 ms, CBV accuracy is lower (CCC < 0.9) than that achieved using more conventional TRs (1–1.5 s). However, for "1 + 1" dosing and the optimal low FA scheme, the CCC exceeds 0.95, even for TRs as low as 500 ms. These results highlight the importance of parameter consistency and encourage caution when applying acceleration techniques.

In Vivo Assessment of Low FA, No Preload DSC-MRI

A recent study was performed to validate in vivo the simulations predicting that single-dose, low-FA DSC-MRI acquisitions without preload ("0 + 1" dosing) give rCBV estimates practically equivalent to the double-dose, intermediate-FA reference standard using full-dose preload ("1 + 1" dosing).[82] Eighty-four patients with a contrast-enhancing brain lesion were included in this 4-institution study. As shown in Fig. 5B, the study demonstrated practical equivalence between the 2 methods, supporting the idea that this low-dose approach should be considered for consensus protocol recommendation, at least at 3 T. The agreement between the two methods was poor if post-processing leakage correction (BSW method) was not also applied. Confirmation of equivalence at 1.5 T requires a similar study.

Conclusions from Computational Parameter Analyses and In Vivo Comparison Study

Based on the recent literature, the following conclusions can be drawn regarding DSC-MRI acquisition methodology:

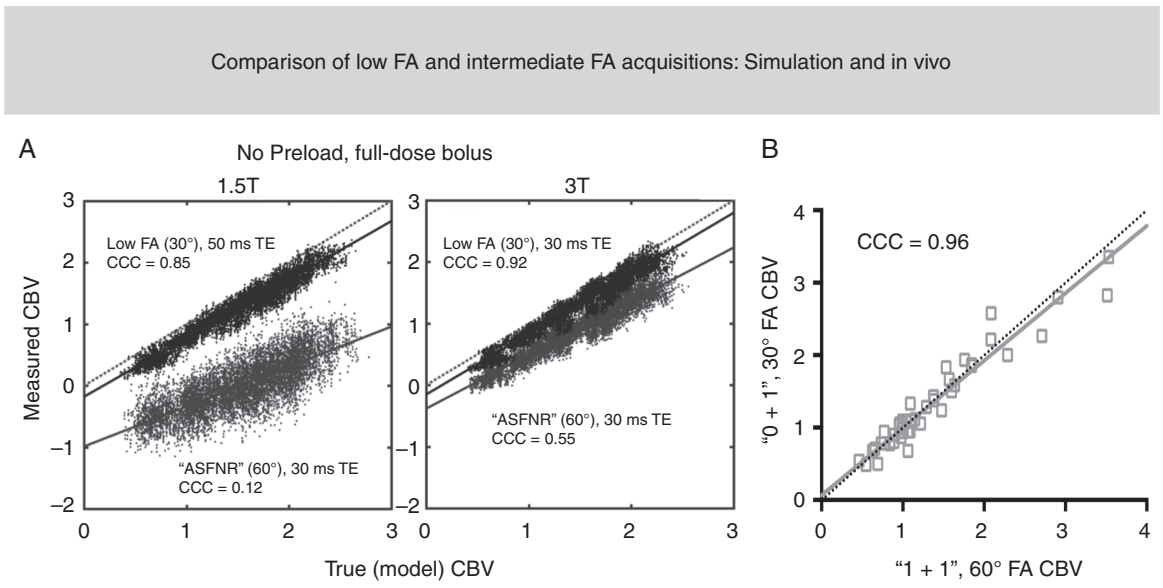

Fig. 5 (A) DRO-based simulations demonstrate that even without preload, low FA (30°) acquisitions give very accurate CBV (along the line of unity) with much less bias compared with intermediate FA (60°) acquisitions, even at 1.5T.[66] (B) Excellent CBV agreement has been observed in vivo at 3T for "0 + 1" and "1 + 1" dosing schemes, according to Lin's concordance correlation (CCC)[82].

1. Of the BTIP-compliant dosing schemes investigated, full-dose preload with full-dose bolus ("1 + 1" dosing) has superior performance, with the least sensitivity to minor pulse sequence parameter fluctuations and the best combination of accuracy and precision, which is important for clinical trials that aim to minimize sample size. Although both low FA (30°) and intermediate FA (60°) sequences provide a high degree of accuracy in simulations testing the "1 + 1" dosing scheme, we continue to consider intermediate FA (60°) to be the gold standard for "1 + 1" dosing, particularly at 3T field strength, given the benefits of higher contrast-to-noise ratio (CNR) and lower sensitivity to parameter variations (eg, TE, TR) compared with low FA (30°) acquisitions.
2. When the "1 + 1" dosing scheme is not desirable (eg, when prioritizing low GBCA dosage), the no-preload paradigm ("0 + 1" dosing) with low FA (30°) and an optimally selected and field-strength dependent TE provides an excellent practical alternative to the gold standard and is the recommended alternative method, particularly at 3T for which in vivo validation has been performed. Based on simulation testing of the "0 + 1" dosing scheme, low FA (30°) acquisitions provide superior accuracy and precision compared with the intermediate FA (60°). This appears to hold true at both 1.5T and 3T field strengths (though has not yet been validated in vivo at 1.5 T).
3. For both the "1 + 1" dosing at intermediate FA (60°) and "0 + 1" dosing at low FA (30°), there is a modest theoretical performance advantage at 3T versus 1.5 T.
4. For BTIP-compliant fractional dosing (eg, "½ + ½" and "¼ + ¾" dosing schemes), a low FA (30°) acquisition should be used at all field strengths, given the superior accuracy and precision compared with intermediate FA (60°) acquisitions, with TE = 30–50 ms having theoretical advantages, especially at 1.5T. However, these fractional dosing schemes likely have poorer performance than the "0 + 1" dosing scheme and the gold-standard "1 + 1" dosing scheme, due to the theoretical costs of poor CNR for fractional bolus dosing, particularly for perfusion metrics such as cerebral blood flow (CBF) and MTT.
5. Post-processing leakage correction is always beneficial, even for low FA (30°) acquisitions, and should be utilized in routine practice.

Time-Point Specifications

Number of Baseline Time Points

Because the number of baseline acquisitions impacts CBV map SNR, image acquisition should begin at least 30–50 time points before contrast injection via a power injector.[67]

Number of Post-Bolus Time Points

Post-processing leakage-correction algorithms and PSR analysis utilize post-bolus "tail" signal intensities, necessitating acquisition of sufficient post-bolus time points. Shown by simulation were 120 total time points (for a typical TR of 1.0–1.5 s) to yield optimal results using the BSW post-processing leakage correction methodology and a 30–50 time point baseline.[66] For longer total acquisitions (eg, 180 time points), reflux of contrast agent back into blood vessels is more likely to occur, violating

assumptions of unidirectional contrast agent efflux.[8] In such cases, bidirectional contrast agent leakage correction schemes are more accurate,[47] with similar accuracy for unidirectional and bidirectional leakage correction when 120 total time points are acquired.[66]

Compatibility with DCE-MRI

When acquisition of both dynamic contrast enhanced (DCE)- and DSC-MRI is desired for a single exam, DCE-MRI is typically performed using the preload dose for DSC-MRI. Preload-based, BTIP-compliant dosing strategies that have been previously evaluated include the "1 + 1" and "½ + ½" protocols. Due to the higher CNR of full-dose acquisitions, the "1 + 1" dosing scheme provides superior DCE- and DSC-parameter accuracy and precision. However, as highlighted in Fig. 4, the "½ + ½" protocol with low FA (30°) provides a reasonable alternative with a modest reduction in accuracy and precision. It is important to note that although the DSC-MRI preload could be used for DCE-MRI, dosage needs to be guided by both DCE-MRI requirements and BTIP compliance, and further investigation is required for determining the fidelity and clinical utility for candidate dosing strategies.

Summary of Updated Recommendations for DSC-MRI Parameters

In light of the emergence of the BTIP standards,[30] recent computer simulation results,[66,81] and multisite in vivo validation,[82] our committee is proposing several modifications to the previously published ASFNR recommendations. Because adoption of DSC-MRI is anticipated for multisite trials, our modified DSC-MRI protocol is BTIP compliant, imposing constraints on contrast agent preload and bolus selection.

From a theoretical perspective, a full-dose preload, full-dose bolus dosing scheme ("1 + 1"), using low (30°) or intermediate (60°) FA and field strength-dependent TE (40-50 ms at 1.5 T, 25-35 ms at 3 T) provides overall best performance based upon accuracy and precision estimates. In clinical trials or at independent clinical sites where double contrast agent dose is acceptable and highest performance is desired, the double-dose ("1 + 1") approach can be used. However, when single-dose GBCA usage is desired or required, we recommend a no-preload, full-dose bolus dosing scheme ("0 + 1") using low FA (30°) and field strength-dependent TE (40-50 ms at 1.5 T, 25-35 ms at 3 T). For most typical applications and with excellent performance preservation, the "0 + 1" approach has advantages, including reduced GBCA usage, as well as elimination of potential systematic error introduced by variation in incubation time between preload and bolus administrations. Although the no-preload, low-FA scheme has slightly poorer accuracy and precision than the full-dose preload, full-dose bolus scheme, the "1 + 1" scheme uses more GBCA, and that downside may more than outweigh the slight gain in performance. Even the fractional dosing schemes ("¼ + ¾" and "½ + ½"), with near equivalent performance using low FA, still have the disadvantage of requiring preload, and potential variation in incubation times can lead to systematic errors. Therefore, the no-preload "0 + 1" protocol may be most appropriate for routine clinical use.

Post-processing leakage correction is beneficial, even for low FA (30°) acquisitions, and should be utilized in routine practice. The BSW method is an advisable technique

Table 2 Summary of protocol recommendations for BTIP-compliant DSC-MRI

Parameter	3T Recommendations (Range)	1.5T Recommendations (Range)
Pulse sequence	GRE-EPI	
Plane	Axial (Oblique Axial)	
Mode	2D	
Dosing protocol (preload + bolus)	"1 + 1": Optimal performance (Preload → T1w + C → DSC bolus injection) "0 + 1": Optimal for single total dose (DSC bolus injection → T1w + C)	
Repetition Time (TR) (msec)	1000–1500	
Echo time (TE) (msec)	30 (25–35) for 30° FA 30 (20–35) for 60° FA	45 (40–50)
Flip angle (FA) (deg)	60 (60–65) or 30 (30–35) ("1 + 1" dosing) 30 (30–35) ("0 + 1" dosing)	
Total time points	≥120	
Baseline time points	50 (30–50)	
Field of view (mm)	(220–240)	
Acquisition matrix	128 × 128 (96–128 × 96–128)	≥96 × 96 (96–128 × 96–128)
Slice thickness (mm)	3 (3–5), as needed for tumor coverage	4 (4–5), as needed for tumor coverage
Slice gap (mm)	0 (0–1), as needed for tumor coverage	
Parallel imaging (GRAPPA/SENSE/CAIPI)	≤2×	
Post-processing leakage correction	Model-based BSW (*unidirectional, or bidirectional for >120 time points*)	

for performing post-processing model-based leakage correction and has thus far the most computer simulation and clinical evidence to support its utility. In the absence of universal acceptance of a single software implementation for widespread use, a benchmark may be required for validating independent DSC-MRI post-processing tools, such as the DRO methodology referenced above.

The updated DSC-MRI protocol recommendations are summarized in Table 2. Integrated BTIP and DSC-MRI protocols for the "0 + 1" and "1 + 1" dosing schemes are summarized in Supplementary Table 1 and Table 2, respectively.

As a final thought, it is worth noting that although the updated DSC-MRI protocol is motivated by theory, computer simulations, in vivo studies, and clinical trial data related to high-grade gliomas, the principles apply to any contrast-enhancing brain lesion, including metastases and active inflammation or infection. Therefore, we believe that the protocol recommendations herein are generally applicable to routine clinical practice.

Supplementary Material

Supplementary data are available at *Neuro-Oncology* online.

Funding

This work was supported by U01 CA176110 (Sponsored by NIH) (KMS), R01 CA 082500 (Sponsored by NIH) (KMS), Medical College of Wisconsin Cancer Center (KMS), R01 CA221938 (Sponsored by NIH) (JLB, CCQ, LSH, KMS), R01 CA213158-01 (Sponsored by NIH) (CCQ), American Cancer Society (ACS) Research Scholar Grant (RSG-15-003-01-CCE) (Ellingson); American Brain Tumor Association (ABTA) Research Collaborators Grant (ARC1700002)(Ellingson); National Brain Tumor Society (NBTS) Research Grant (Ellingson, Cloughesy); NIH/NCI UCLA Brain Tumor SPORE (1P50CA211015-01A1) (Ellingson, Cloughesy); NIH/NCI 1R21CA223757-01 (Ellingson)

Conflict of interest statement

Past ownership interest and current financial interest in Imaging Biometrics LLC (KMS) and ownership interest in IQ-AI Ltd (KMS).

Acknowledgments

We would like to thank additional members of the Jumpstarting Brain Tumor Drug Development Coalition Imaging Standardization Steering Committee including David F. Arons and Ann Kingston from the National Brain Tumor Society (NBTS), Boston, MA, David Sandak and Max Wallace from the Accelerate Brain Cancer Cure (ABC^2), Washington, D.C., Al Musella from the Musella Foundation, Hewlett, NY, and Chas Haynes from the Collaborative Ependymoma Research Network, Dayton, OH.

References

1. Rosen BR, Belliveau JW, Vevea JM, Brady TJ. Perfusion imaging with NMR contrast agents. *Magn Reson Med.* 1990;14(2):249–265.
2. Belliveau JW, Kennedy DN Jr, McKinstry RC, et al. Functional mapping of the human visual cortex by magnetic resonance imaging. *Science.* 1991;254(5032):716–719.
3. Aronen HJ, Gazit IE, Louis DN, et al. Cerebral blood volume maps of gliomas: comparison with tumor grade and histologic findings. *Radiology.* 1994; 191(1):41–51.
4. Maeda M, Itoh S, Kimura H, et al. Tumor vascularity in the brain: evaluation with dynamic susceptibility-contrast MR imaging. *Radiology.* 1993; 189(1):233–238.
5. Donahue KM, Krouwer HG, Rand SD, et al. Utility of simultaneously acquired gradient-echo and spin-echo cerebral blood volume and morphology maps in brain tumor patients. *Magn Reson Med.* 2000;43(6):845–853.
6. Aronen HJ, Pardo FS, Kennedy DN, et al. High microvascular blood volume is associated with high glucose uptake and tumor angiogenesis in human gliomas. *Clin Cancer Res.* 2000;6(6):2189–2200.
7. Sugahara T, Korogi Y, Kochi M, Ushio Y, Takahashi M. Perfusion-sensitive MR imaging of gliomas: comparison between gradient-echo and spin-echo echo-planar imaging techniques. *AJNR Am J Neuroradiol.* 2001;22(7):1306–1315.
8. Boxerman JL, Schmainda KM, Weisskoff RM. Relative cerebral blood volume maps corrected for contrast agent extravasation significantly correlate with glioma tumor grade, whereas uncorrected maps do not. *AJNR Am J Neuroradiol.* 2006;27(4):859–867.
9. Law M, Oh S, Babb JS, et al. Low-grade gliomas: dynamic susceptibility-weighted contrast-enhanced perfusion MR imaging—prediction of patient clinical response. *Radiology.* 2006;238(2):658–667.
10. Jiang Z, Le Bas JF, Grand S, et al. Prognostic value of perfusion MR imaging in patients with oligodendroglioma: a survival study. *J Neuroradiol.* 2011;38(1):53–61.
11. Hipp SJ, Steffen-Smith E, Hammoud D, Shih JH, Bent R, Warren KE. Predicting outcome of children with diffuse intrinsic pontine gliomas using multiparametric imaging. *Neuro Oncol.* 2011;13(8):904–909.
12. Bonekamp D, Deike K, Wiestler B, et al. Association of overall survival in patients with newly diagnosed glioblastoma with contrast-enhanced perfusion MRI: comparison of intraindividually matched T1 - and T2 (*)-based bolus techniques. *J Magn Reson Imaging.* 2015;42(1):87–96.
13. Jabehdar Maralani P, Melhem ER, Wang S, et al. Association of dynamic susceptibility contrast enhanced MR perfusion parameters with prognosis in elderly patients with glioblastomas. *Eur Radiol.* 2015;25(9):2738–2744.
14. Barajas RF Jr, Chang JS, Segal MR, et al. Differentiation of recurrent glioblastoma multiforme from radiation necrosis after external beam radiation therapy with dynamic susceptibility-weighted contrast-enhanced perfusion MR imaging. *Radiology.* 2009;253(2):486–496.
15. Hu LS, Baxter LC, Smith KA, et al. Relative cerebral blood volume values to differentiate high-grade glioma recurrence from posttreatment radiation effect: direct correlation between image-guided tissue histopathology and localized dynamic susceptibility-weighted contrast-enhanced perfusion MR imaging measurements. *AJNR Am J Neuroradiol.* 2009;30(3):552–558.
16. Gasparetto EL, Pawlak MA, Patel SH, et al. Posttreatment recurrence of malignant brain neoplasm: accuracy of relative cerebral blood volume fraction in discriminating low from high malignant histologic volume fraction. *Radiology.* 2009;250(3):887–896.

17. Kim HS, Goh MJ, Kim N, Choi CG, Kim SJ, Kim JH. Which combination of MR imaging modalities is best for predicting recurrent glioblastoma? Study of diagnostic accuracy and reproducibility. *Radiology.* 2014;273(3):831–843.
18. Hu LS, Eschbacher JM, Heiserman JE, et al. Reevaluating the imaging definition of tumor progression: perfusion MRI quantifies recurrent glioblastoma tumor fraction, pseudoprogression, and radiation necrosis to predict survival. *Neuro Oncol.* 2012;14(7):919–930.
19. Young RJ, Gupta A, Shah AD, et al. MRI perfusion in determining pseudoprogression in patients with glioblastoma. *Clin Imaging.* 2013;37(1):41–49.
20. Schmainda KM, Prah M, Connelly J, et al. Dynamic-susceptibility contrast agent MRI measures of relative cerebral blood volume predict response to bevacizumab in recurrent high-grade glioma. *Neuro Oncol.* 2014;16(6):880–888.
21. Leu K, Enzmann DR, Woodworth DC, et al. Hypervascular tumor volume estimated by comparison to a large-scale cerebral blood volume radiographic atlas predicts survival in recurrent glioblastoma treated with bevacizumab. *Cancer Imaging.* 2014;14:31.
22. Aquino D, Di Stefano AL, Scotti A, et al. Parametric response maps of perfusion MRI may identify recurrent glioblastomas responsive to bevacizumab and irinotecan. *PLoS One.* 2014;9(3):e90535.
23. Schmainda KM, Zhang Z, Prah M, et al. Dynamic susceptibility contrast MRI measures of relative cerebral blood volume as a prognostic marker for overall survival in recurrent glioblastoma: results from the ACRIN 6677/RTOG 0625 multicenter trial. *Neuro Oncol.* 2015;17(8):1148–1156.
24. Kickingereder P, Wiestler B, Burth S, et al. Relative cerebral blood volume is a potential predictive imaging biomarker of bevacizumab efficacy in recurrent glioblastoma. *Neuro Oncol.* 2015;17(8):1139–1147.
25. Harris RJ, Cloughesy TF, Hardy AJ, et al. MRI perfusion measurements calculated using advanced deconvolution techniques predict survival in recurrent glioblastoma treated with bevacizumab. *J Neurooncol.* 2015;122(3):497–505.
26. Geer CP, Simonds J, Anvery A, et al. Does MR perfusion imaging impact management decisions for patients with brain tumors? A prospective study. *AJNR Am J Neuroradiol.* 2012;33(3):556–562.
27. Willats L, Calamante F. The 39 steps: evading error and deciphering the secrets for accurate dynamic susceptibility contrast MRI. *NMR Biomed.* 2013;26(8):913–931.
28. Semmineh NB, Xu J, Skinner JT, et al. Assessing tumor cytoarchitecture using multiecho DSC-MRI derived measures of the transverse relaxivity at tracer equilibrium (TRATE). *Magn Reson Med.* 2015;74(3):772–784.
29. Stokes AM, Skinner JT, Yankeelov T, Quarles CC. Assessment of a simplified spin and gradient echo (sSAGE) approach for human brain tumor perfusion imaging. *Magn Reson Imaging.* 2016;34(9):1248–1255.
30. Ellingson BM, Bendszus M, Boxerman J, et al; Jumpstarting Brain Tumor Drug Development Coalition Imaging Standardization Steering Committee. Consensus recommendations for a standardized Brain Tumor Imaging Protocol in clinical trials. *Neuro Oncol.* 2015;17(9):1188–1198.
31. Meier P, Zierler KL. On the theory of the indicator-dilution method for measurement of blood flow and volume. *J Appl Physiol.* 1954;6(12):731–744.
32. Villringer A, Rosen BR, Belliveau JW, et al. Dynamic imaging with lanthanide chelates in normal brain: contrast due to magnetic susceptibility effects. *Magn Reson Med.* 1988;6(2):164–174.
33. Rempp KA, Brix G, Wenz F, Becker CR, Gückel F, Lorenz WJ. Quantification of regional cerebral blood flow and volume with dynamic susceptibility contrast-enhanced MR imaging. *Radiology.* 1994;193(3):637–641.
34. Bedekar D, Jensen T, Schmainda KM. Standardization of relative cerebral blood volume (rCBV) image maps for ease of both inter- and intrapatient comparisons. *Magn Reson Med.* 2010;64(3):907–913.
35. Ellingson BM, Zaw T, Cloughesy TF, et al. Comparison between intensity normalization techniques for dynamic susceptibility contrast (DSC)-MRI estimates of cerebral blood volume (CBV) in human gliomas. *J Magn Reson Imaging.* 2012;35(6):1472–1477.
36. Boxerman JL, Hamberg LM, Rosen BR, Weisskoff RM. MR contrast due to intravascular magnetic susceptibility perturbations. *Magn Reson Med.* 1995;34(4):555–566.
37. Fisel CR, Ackerman JL, Buxton RB, et al. MR contrast due to microscopically heterogeneous magnetic susceptibility: numerical simulations and applications to cerebral physiology. *Magn Reson Med.* 1991;17(2):336–347.
38. Schmiedeskamp H, Straka M, Newbould RD, et al. Combined spin- and gradient-echo perfusion-weighted imaging. *Magn Reson Med.* 2012;68(1):30–40.
39. Zama A, Tamura M, Inoue HK. Three-dimensional observations on microvascular growth in rat glioma using a vascular casting method. *J Cancer Res Clin Oncol.* 1991;117(5):396–402.
40. Badruddoja MA, Krouwer HG, Rand SD, Rebro KJ, Pathak AP, Schmainda KM. Antiangiogenic effects of dexamethasone in 9L gliosarcoma assessed by MRI cerebral blood volume maps. *Neuro Oncol.* 2003;5(4):235–243.
41. Weisskoff RM, Zuo CS, Boxerman JL, Rosen BR. Microscopic susceptibility variation and transverse relaxation: theory and experiment. *Magn Reson Med.* 1994;31(6):601–610.
42. Paulson ES, Schmainda KM. Comparison of dynamic susceptibility-weighted contrast-enhanced MR methods: recommendations for measuring relative cerebral blood volume in brain tumors. *Radiology.* 2008;249(2):601–613.
43. Quarles CC, Gochberg DF, Gore JC, Yankeelov TE. A theoretical framework to model DSC-MRI data acquired in the presence of contrast agent extravasation. *Phys Med Biol.* 2009;54(19):5749–5766.
44. Cha S, Knopp EA, Johnson G, Wetzel SG, Litt AW, Zagzag D. Intracranial mass lesions: dynamic contrast-enhanced susceptibility-weighted echo-planar perfusion MR imaging. *Radiology.* 2002;223(1):11–29.
45. Schmainda KM, Rand SD, Joseph AM, et al. Characterization of a first-pass gradient-echo spin-echo method to predict brain tumor grade and angiogenesis. *AJNR Am J Neuroradiol.* 2004;25(9):1524–1532.
46. Quarles CC, Ward BD, Schmainda KM. Improving the reliability of obtaining tumor hemodynamic parameters in the presence of contrast agent extravasation. *Magn Reson Med.* 2005;53(6):1307–1316.
47. Leu K, Boxerman JL, Lai A, et al. Bidirectional Contrast agent leakage correction of dynamic susceptibility contrast (DSC)-MRI improves cerebral blood volume estimation and survival prediction in recurrent glioblastoma treated with bevacizumab. *J Magn Reson Imaging.* 2016;44(5):1229–1237.
48. Paulson ES, Prah DE, Schmainda KM. Spiral perfusion imaging with consecutive echoes (SPICE™) for the simultaneous mapping of DSC- and DCE-MRI parameters in brain tumor patients: theory and initial feasibility. *Tomography.* 2016;2(4):295–307.
49. Vonken EP, van Osch MJ, Bakker CJ, Viergever MA. Simultaneous quantitative cerebral perfusion and Gd-DTPA extravasation measurement with dual-echo dynamic susceptibility contrast MRI. *Magn Reson Med.* 2000;43(6):820–827.
50. Gahramanov S, Muldoon LL, Li X, Neuwelt EA. Improved perfusion MR imaging assessment of intracerebral tumor blood volume and antiangiogenic therapy efficacy in a rat model with ferumoxytol. *Radiology.* 2011;261(3):796–804.
51. Horváth A, Varallyay CG, Schwartz D, et al. Quantitative comparison of delayed ferumoxytol T1 enhancement with immediate gadoteridol enhancement in high grade gliomas. *Magn Reson Med.* 2018;80(1):224–230.

52. Hu LS, Baxter LC, Pinnaduwage DS, et al. Optimized preload leakage-correction methods to improve the diagnostic accuracy of dynamic susceptibility-weighted contrast-enhanced perfusion MR imaging in posttreatment gliomas. *AJNR Am J Neuroradiol.* 2010;31(1):40–48.
53. Weisskoff RM, Boxerman JL, Sorensen AG, Kulke SM, Campbell TA, Rosen BR. Simultaneous blood volume and permebility mapping using a single Gd-based contrast injection. Paper presented at: Society of Magnetic Resonance in Medicine, 2nd Annual Meeting; 1994; San Francisco, CA.
54. Bjornerud A, Sorensen AG, Mouridsen K, Emblem KE. T1- and T2*-dominant extravasation correction in DSC-MRI: part I—theoretical considerations and implications for assessment of tumor hemodynamic properties. *J Cereb Blood Flow Metab.* 2011;31(10):2041–2053.
55. Leu K, Boxerman JL, Cloughesy TF, et al. Improved leakage correction for single-echo dynamic susceptibility contrast perfusion MRI estimates of relative cerebral blood volume in high-grade gliomas by accounting for bidirectional contrast agent exchange. *AJNR Am J Neuroradiol.* 2016;37(8):1440–1446.
56. Welker K, Boxerman J, Kalnin A, Kaufmann T, Shiroishi M, Wintermark M; American Society of Functional Neuroradiology MR Perfusion Standards and Practice Subcommittee of the ASFNR Clinical Practice Committee. ASFNR recommendations for clinical performance of MR dynamic susceptibility contrast perfusion imaging of the brain. *AJNR Am J Neuroradiol.* 2015;36(6):E41–E51.
57. Boxerman JL, Prah DE, Paulson ES, Machan JT, Bedekar D, Schmainda KM. The role of preload and leakage correction in gadolinium-based cerebral blood volume estimation determined by comparison with MION as a criterion standard. *AJNR Am J Neuroradiol.* 2012;33(6):1081–1087.
58. Hu LS, Eschbacher JM, Dueck AC, et al. Correlations between perfusion MR imaging cerebral blood volume, microvessel quantification, and clinical outcome using stereotactic analysis in recurrent high-grade glioma. *AJNR Am J Neuroradiol.* 2012;33(1):69–76.
59. Prah MA, Al-Gizawiy MM, Mueller WM, et al. Spatial discrimination of glioblastoma and treatment effect with histologically-validated perfusion and diffusion magnetic resonance imaging metrics. *J Neurooncol.* 2018;136(1):13–21.
60. Prah MA, Stufflebeam SM, Paulson ES, et al. Repeatability of standardized and normalized relative CBV in patients with newly diagnosed glioblastoma. *AJNR Am J Neuroradiol.* 2015;36(9):1654–1661.
61. Gerstner ER, Zhang Z, Fink JR, et al; ACRIN 6684 Trial Group. ACRIN 6684: assessment of tumor hypoxia in newly diagnosed glioblastoma using 18F-FMISO PET and MRI. *Clin Cancer Res.* 2016;22(20):5079–5086.
62. Hu LS, Kelm Z, Korfiatis P, et al. Impact of software modeling on the accuracy of perfusion MRI in glioma. *AJNR Am J Neuroradiol.* 2015;36(12):2242–2249.
63. Bell LC, Semmineh N, An H, et al. Evaluating multisite rCBV consistency from DSC-MRI imaging protocols and postprocessing software across the NCI quantitative imaging network sites using a digital reference object (DRO). *Tomography.* 2019;5(1):110–117.
64. Schmainda KM, Prah MA, Rand SD, et al. Multisite concordance of DSC-MRI analysis for brain tumors: results of a national cancer institute quantitative imaging network collaborative project. *AJNR Am J Neuroradiol.* 2018;39(6):1008–1016.
65. Semmineh NB, Stokes AM, Bell LC, Boxerman JL, Quarles CC. A population-based digital reference object (DRO) for optimizing dynamic susceptibility contrast (DSC)-MRI methods for clinical trials. *Tomography.* 2017;3(1):41–49.
66. Semmineh NB, Bell LC, Stokes AM, Hu LS, Boxerman JL, Quarles CC. Optimization of acquisition and analysis methods for clinical dynamic susceptibility contrast MRI using a population-based digital reference object. *AJNR Am J Neuroradiol.* 2018;39(11):1981–1988.
67. Boxerman JL, Rosen BR, Weisskoff RM. Signal-to-noise analysis of cerebral blood volume maps from dynamic NMR imaging studies. *J Magn Reson Imaging.* 1997;7(3):528–537.
68. Thilmann O, Larsson EM, Björkman-Burtscher IM, Ståhlberg F, Wirestam R. Effects of echo time variation on perfusion assessment using dynamic susceptibility contrast MR imaging at 3 tesla. *Magn Reson Imaging.* 2004;22(7):929–935.
69. Knutsson L, Ståhlberg F, Wirestam R. Aspects on the accuracy of cerebral perfusion parameters obtained by dynamic susceptibility contrast MRI: a simulation study. *Magn Reson Imaging.* 2004;22(6):789–798.
70. Smith MR, Lu H, Frayne R. Signal-to-noise ratio effects in quantitative cerebral perfusion using dynamic susceptibility contrast agents. *Magn Reson Med.* 2003;49(1):122–128.
71. Barajas RF Jr, Hodgson JG, Chang JS, et al. Glioblastoma multiforme regional genetic and cellular expression patterns: influence on anatomic and physiologic MR imaging. *Radiology.* 2010;254(2):564–576.
72. Das S, Marsden PA. Angiogenesis in glioblastoma. *N Engl J Med.* 2013;369(16):1561–1563.
73. Brandsma D, van den Bent MJ. Pseudoprogression and pseudoresponse in the treatment of gliomas. *Curr Opin Neurol.* 2009;22(6):633–638.
74. Wen PY, Macdonald DR, Reardon DA, et al. Updated response assessment criteria for high-grade gliomas: response assessment in neuro-oncology working group. *J Clin Oncol.* 2010;28(11):1963–1972.
75. Prager AJ, Martinez N, Beal K, Omuro A, Zhang Z, Young RJ. Diffusion and perfusion MRI to differentiate treatment-related changes including pseudoprogression from recurrent tumors in high-grade gliomas with histopathologic evidence. *AJNR Am J Neuroradiol.* 2015;36(5):877–885.
76. Mangla R, Singh G, Ziegelitz D, et al. Changes in relative cerebral blood volume 1 month after radiation-temozolomide therapy can help predict overall survival in patients with glioblastoma. *Radiology.* 2010;256(2):575–584.
77. Kong DS, Kim ST, Kim EH, et al. Diagnostic dilemma of pseudoprogression in the treatment of newly diagnosed glioblastomas: the role of assessing relative cerebral blood flow volume and oxygen-6-methylguanine-DNA methyltransferase promoter methylation status. *AJNR Am J Neuroradiol.* 2011;32(2):382–387.
78. Boxerman JL, Ellingson BM, Jeyapalan S, et al. Longitudinal DSC-MRI for distinguishing tumor recurrence from pseudoprogression in patients with a high-grade glioma. *Am J Clin Oncol.* 2017;40(3):228–234.
79. Patel P, Baradaran H, Delgado D, et al. MR perfusion-weighted imaging in the evaluation of high-grade gliomas after treatment: a systematic review and meta-analysis. *Neuro Oncol.* 2017;19(1):118–127.
80. Ostergaard L, Weisskoff RM, Chesler DA, Gyldensted C, Rosen BR. High resolution measurement of cerebral blood flow using intravascular tracer bolus passages. Part I: mathematical approach and statistical analysis. *Magn Reson Med.* 1996;36(5):715–725.
81. Leu K, Boxerman JL, Ellingson BM. Effects of MRI protocol parameters, preload injection dose, fractionation strategies, and leakage correction algorithms on the fidelity of dynamic-susceptibility contrast mri estimates of relative cerebral blood volume in gliomas. *AJNR Am J Neuroradiol.* 2017;38(3):478–484.
82. Schmainda KM, Prah MA, Hu LS, et al. Moving Toward a Consensus DSC-MRI Protocol: Validation of a Low-Flip Angle Single-Dose Option as a Reference Standard for Brain Tumors. *AJNR Am J Neuroradiol.* 2019;40(4):626–633.